Available online at www.sciencedirect.com
SCIENCE DIRECT
Polymer 46 (2005) 5225–5231
polymer
www.elsevier.com/locate/polymer

Nanostructural physical and chemical information derived from the unit cell scattering amplitudes of a spider dragline silk

J.E. Trancik[a,b], J.T. Czernuszka[a], D.J.H. Cockayne[a], C. Viney[a,c,*]

[a]*Department of Materials, University of Oxford, Parks Road, Oxford OX1 3PH, UK*
[b]*Earth Institute, Columbia University, New York, NY 10025, USA*
[c]*School of Engineering, University of California at Merced, P.O. Box 2039, Merced, CA 95344, USA*

Received 18 December 2004; received in revised form 1 April 2005; accepted 4 April 2005
Available online 5 May 2005

Abstract

Characterizing the nanostructures of spider major ampullate (dragline) silks is an important step in understanding the origin of their high mean strength and toughness, and for producing polymeric analogs that mimic these properties. Here we present transmission electron microscopy (TEM) diffraction patterns and an accompanying structure factor analysis for the dragline silk of *Latrodectus hesperus* (black widow spider). The chemical and physical composition of crystalline regions in this silk fiber was studied by manipulating the positions and size of amino acid side groups in a theoretical model, and comparing the expected unit cell scattering amplitudes with experimental electron diffraction patterns. The results suggest that—in addition to the smaller amino acid side groups such as alanine, glycine and serine—some of the bulkier amino acid side groups such as tyrosine and leucine are included in the crystalline fraction of the major ampullate silk. The structure factor analysis also demonstrates a marked sensitivity of the respective diffraction spot intensities to a slight change in both side group position and side group bulkiness. These observations point to a unique function for TEM in characterizing silk and other polymers.

Keywords: Electron diffraction; Silk; Structure factor

1. Introduction

Spider dragline silks are high performance natural polymers that, unlike many artificial polymers, are synthesized at room temperature and without the use of polluting petrochemicals. There is considerable scientific and commercial interest in being able to produce silk analogs that mimic the high mean breaking strength and toughness of the natural polymer, and that are environmentally friendly to manufacture [1]. While analogs have been synthesized in genetically modified host organisms as varied as tobacco [2], potato [2] and mammalian cells [3], these have not yet succeeded in reliably replicating the strength and toughness of natural silk. Furthermore, the impressive tensile properties of native dragline as revealed in constant strain rate tests are compromised by creep and stress relaxation [4–6], which in turn are exacerbated by moisture [4,6]; the adoption of silk analogs as an engineering material will depend on how well these limitations can be overcome.

To achieve high mechanical performance in silk analogs, an understanding of the complex physical and chemical structure of native spider silks at all pertinent length scales is required. Currently, significant gaps remain in the necessary comprehensive characterization of structure. Knowledge of the microstructural and nanostructural features, the processing conditions that realize these, and in turn how these give rise to silks' unique mechanical properties is important for our ability to synthesize analogs with comparable or enhanced mechanical properties; it is also needed to further our understanding of the fundamental scientific principles that govern the performance of the native polymer. Relating the microstructure to observed mechanical properties is beyond the scope of this paper but will be addressed elsewhere [7].

Several of the important early studies of silk focused on silkworm silk. Warwicker [8] and Marsh et al. [9–11]

* Corresponding author. Address: School of Engineering, University of California at Merced, P.O. Box 2039, Merced, CA 95344, USA. Tel.: +1 209 724 4359; fax: +1 209 724 2912.
E-mail address: cviney@ucmerced.edu (C. Viney).

0032-3861/$ - see front matter © 2005 Elsevier Ltd. All rights reserved.
doi:10.1016/j.polymer.2005.04.007

published X-ray diffraction (XRD) studies of *Bombyx mori* (silkworm) silk that revealed a highly ordered structure compared with other fibrous proteins. Marsh et al. derived a β-sheet structure and an orthogonal unit cell which they termed a pseudo-cell, stating that because the crystalline portions cannot be assumed to contain only the smallest amino acids (glycine, alanine and serine), the intersheet dimension may be extended in certain regions in order to accommodate larger residues such as tyrosine and leucine. Warwicker subsequently characterized a number of insect and spider silks, again using XRD; he found that, while the unit cells are all orthogonal, the intersheet distances vary from one silk to the next [12,13]. All the silks that Warwicker studied have the same dipeptide (fiber axis) dimension, and the same interchain dimension within β-sheets.

More recent XRD diffraction studies of various spider dragline silks have provided further evidence of a β-sheet structure and orthogonal unit cell [14,15]; these studies have also determined crystal sizes of ca. 2–7 nm, with longer dimensions oriented along the fiber axis. The crystals are thought to be composed primarily of polyalanine and embedded in an amorphous or semi-amorphous matrix containing some of the larger amino acids. NMR studies of the dragline silk of *Nephila edulis* have, however, indicated that some glycine residues are incorporated into the β-sheet structure [16].

Single crystal diffraction patterns and dark field images have been reported from transmission electron microscopy (TEM) studies of *Nephila clavipes* dragline silk, indicating the presence of crystals ranging from 70 to 500 nm in size [17,18]. These were termed non-periodic lattice (NPL) crystals; the protein backbones contribute the 'lattice' and 'crystal' attributes, while the amino acid side chains confer the 'non-periodic' characteristics. NPL crystals are described as regions in which the local composition imparted by the amino acid side chains is variable, as, therefore, are the local intersheet spacing and the degree of order defined by the number of nearest-neighbor matches between amino acid residues on adjacent chains within β-sheets. The NPL crystals model allows for the presence of small, perfect polyalanine crystals embedded in imperfect areas that contain glycine and some of the other, larger, residues.

Here we present a structure factor analysis of TEM diffraction patterns from *Latrodectus hesperus* dragline silk. The structure factor analysis provides a tool for probing the chemical composition of the crystals in silk based on the observed scattering intensities for specific crystal planes. Despite the beam sensitivity of silk specimens, TEM is proving to be a useful tool for examining both physical and chemical aspects of their complex structure. TEM provides access to this information at down to nanometer length scales, as well as the ability to record both polycrystalline and single crystal diffraction patterns.

2. Methods

The method for collecting silk samples and preparing TEM specimens is described in detail elsewhere [19]. The procedure involves collecting dragline silk from an adult female *L. hesperus* around a rotating wheel. The silk is then rewound around a polyester film to control sample orientation, and the silk and film are then embedded in epoxy resin (TAAB Embedding Resin) and cured at 60 °C for 24 h. Sections of 60–90 nm thickness are cut with a diamond knife on a Sorvall Ultra Microtome MT500, and then transferred to 3 mm diameter, 400 mesh TEM copper grids.

Specimens were examined with a JEOL 4000EX CETEM, equipped with a liquid nitrogen cooling stage and operating at 400 keV. The cooling system was held at −120 °C, the lowest temperature at which ice crystals did not form. To increase the working time before specimen degradation, high accelerating voltages and low beam intensities were used, together with other low-dose imaging techniques [20]. As a result of the low beam intensities required, diffraction patterns and dark field images were not easily resolvable on the screen and only became visible in the developed negative [21].

In analysis of TEM diffraction patterns, reflection spacings were measured visually from magnified negatives, and digitally, in order to verify the peak position of the radially-averaged intensity. A gold standard was used to calibrate the camera length. To determine unit cell dimensions and index the diffraction patterns, the intersheet distance was treated as an unknown variable and iteratively refined, while the interchain and dipeptide spacings in the orthogonal unit cell were set equal to the values consistently obtained from other silks [12,13].

3. Results and discussion

Polycrystalline patterns showing a preferred orientation were recorded from longitudinal cross-sections of dragline silk, as were single crystal diffraction patterns (Figs. 1 and 2). The broadening of intensity maxima in diffraction patterns suggests the presence of crystals in the 2 nm size range (detected in polycrystalline patterns) and isolated crystals ranging in size from 40 to 120 nm (detected in single crystal diffraction patterns). A detailed discussion of crystal size determination, and of the existence of a bimodal crystal size distribution as detected in TEM and also XRD studies, is presented elsewhere [7,21].

There is limited information available on the primary structure and therefore the unit cell of crystals in *L. hesperus* dragline silk. A study of mole percent amino acid composition has been published which indicates a similarity to the percent composition of *Nephila clavipes* dragline silk [22]. Moreover, the structural repeats along the polypeptide backbone and perpendicular to the backbone in the plane of

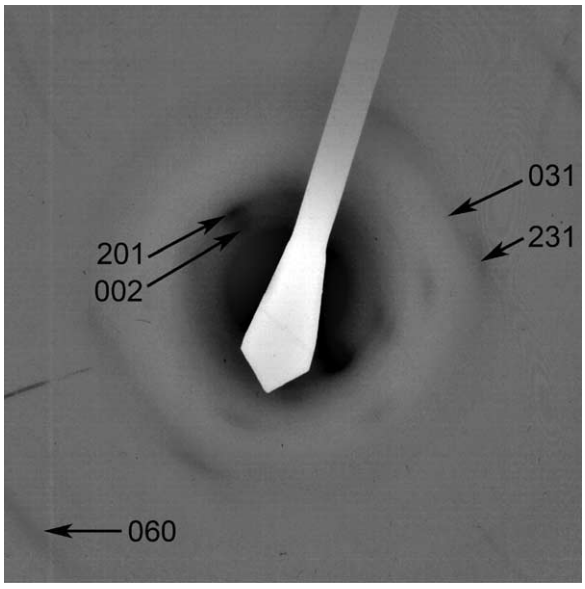

Fig. 1. Polycrystalline electron diffraction pattern, recorded from a longitudinal section of *L. hesperus* dragline silk and exhibiting a fiber texture. The molecular backbone is approximately parallel to the fiber axis. The proximity of *d*-spacings for (102) and (201) planes, equal to 0.47 and 0.43 nm, respectively, causes some uncertainty in the indexing of the 201 reflection. The 201 indices provide the closest match.

a β-sheet are known from previous work to be conserved in a wide range of spider and insect silks [12]. Our XRD studies [7,21] demonstrate that these two unit cell dimensions are also conserved in *L. hesperus* dragline. The identity of amino acid side groups—and thus the structural repeat in the intersheet direction—has, however, been shown to vary from one silk to the next. Both XRD and electron diffraction [7,21] were used to measure this

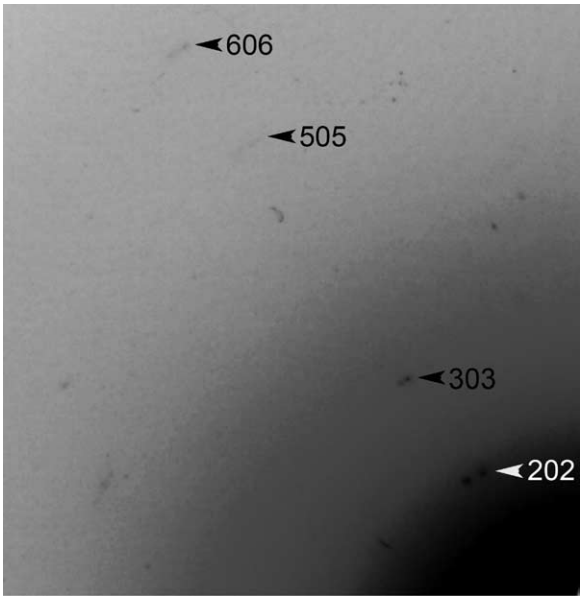

Fig. 2. Single crystal electron diffraction pattern recorded from a longitudinal section of *L. hesperus* dragline silk. Spots are indexed if there is a unique match.

parameter for *L. hesperus* dragline. The lattice parameters for the orthogonal unit cell of *L. hesperus* dragline are: $a=$ 0.94 nm (interchain); $b=0.70$ nm (dipeptide, chain direction); $c=1.08$ nm (intersheet). (Although it is common in polymer fiber diffraction studies to assign the unit cell *c*-axis to the chain direction, we have chosen here to assign the unit cell *b*-axis to this direction. This choice is motivated by the crystallographic convention that space group $P2_1$—which describes the unit cell symmetry of imperfectly crystalline NPL regions in spider dragline, where the screw axis lies parallel to the chains [18]—assigns the unique axis to be oriented along *b*). Streaking in some single crystal diffraction patterns suggests lattice strains. These strains are likely to occur in the intersheet direction, where the distance is governed by van der Waals packing of side chain moieties and so is variable between silks and even within a single NPL crystal in a given silk.

The diffraction patterns in Figs. 1 and 2 were used for the purpose of the structure factor analysis. The diffraction spots and arcs are faint, due to weak scattering and the low beam intensity that is required to avoid rapid degradation. The structure factor analysis was performed using available information on the arrangement of atoms along the polypeptide backbone and perpendicular to it, and assigning possible side groups to the β-sheets to observe how these affect the predicted relative intensities of reflections. Two general cases were considered: (1) identical side groups; and (2) varied side groups.

Several different space groups have been proposed for *B. mori* and spider silks, depending on the symmetry of the particular structural features that were considered: $P2_1$, $P2_12_12$, and $P2_12_12_1$ [8,9,18]. These correspond to one, two, and three orthogonal screw axes, respectively, and their applicability to different silks depends on the identity of side groups. Forbidden reflections for each of these three space groups are: $0k0$: $k=2n+1$ ($P2_1$); $h00$: $h=2n+1$, $0k0$: $k=2n+1$ ($P2_12_12$); $h00$: $h=2n+1$, $0k0$: $k=2n+1$, $00l$: $l=2n+1$ ($P2_12_12_1$) [23]. Although none of the forbidden reflections were observed in the diffraction patterns obtained in the present study, we cannot be certain whether these reflections were systematically absent due to symmetry, or merely absent (or extremely weak) as a result of the particular unit cell contents. For the present analysis of *L. hesperus* dragline silk the side groups are not known. Therefore, the space group $P2_1$ was considered in this study; it assumes the least amount of symmetry and thus requires the most general expression for the structure factor.

The unit of structure shown in Fig. 3—determined by Marsh et al. for *B. mori* silk—was used as a starting point [9]. The atom positional parameters are shown in Table 1. The identity and positions of atoms were then modified to account for the cases of identical and dissimilar side groups. Relativistic Hartree–Fock atomic scattering amplitudes (f_j) for electrons were obtained from the International Tables of Crystallography [24]. The structure factor is described by [25].

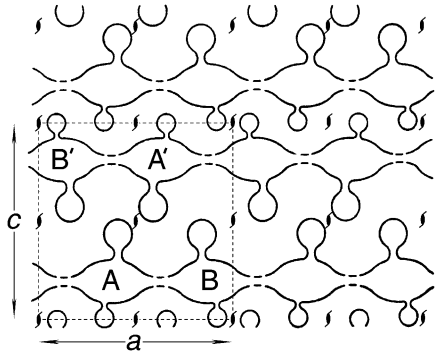

Fig. 3. The 'pseudo' unit of structure proposed by Marsh et al., projected along the fiber axis. Figure adapted from Marsh et al. [9]. Space group: $P2_1$. Equivalent positions: x,y,z (chains A and B); $\bar{x}$, $1/2+y$, $\bar{z}$ (chains A′ and B′). Asymmetric unit: $0\le x\le 1$; $0\le y\le 1$; $0\le z\le 1/2$.

$$F_{hkl} = \sum_j f_j \exp[2\pi i(hx_j + ky_j + lz_j)]$$

which is the general equation for the structure factor—a summation over all atoms j in the unit cell. f_j is the electron atomic scattering factor for atom j; it is a function of scattering angle. x, y, z indicate the positions of atoms. $|F_{hkl}|^2$ corresponds to the expected reflection intensity for the plane with indices h, k and l. The structure factor can be written as the sum of real and imaginary parts:

$$F = A + iB$$

$$|F|^2 = A^2 + B^2$$

For space group $P2_1$ (unique axis b), $k=2n$ gives

$$A_{hkl} = \sum_j 2f_j \cos 2\pi(hx_j + lz_j)\cos 2\pi ky_j$$

$$B_{hkl} = \sum_j 2f_j \cos 2\pi(hx_j + lz_j)\sin 2\pi ky_j$$

And $k=2n+1$ gives

$$A_{hkl} = -\sum_j 2f_j \sin 2\pi(hx_j + lz_j)\sin 2\pi ky_j$$

$$B_{hkl} = \sum_j 2f_j \sin 2\pi(hx_j + lz_j)\cos 2\pi ky_j$$

Table 2 displays the $|F|^2$ values calculated for the case of dissimilar side groups. The structure used here as a starting point is that of *B. mori* silk, i.e. (Gly-Ala-Gly-Ala-Gly-Ser)$_n$. Two simplifications are made, namely: hydrogen atoms are not taken into account—justified by their low scattering factors; and serine is treated as structurally and chemically identical to alanine. (Both simplifications were used by Marsh et al., in calculations based on their pseudo-cell [9]). In effect, the latter simplification changes the amino acid sequence to (Gly-Ala)$_n$, deviating from the *B. mori* sequence. However, this deviation does not impede an investigation of the two general cases named earlier: identical and varied side groups.

Table 3 displays $|F|^2$ values for the case of identical side groups. All side groups contain one carbon atom (alanine). The positions of atoms are the same as shown in Table 1, with the addition of carbon atoms at the positions indicated by italic print.

Comparing Tables 2 and 3 with experimentally obtained intensities (Table 4) indicates that the predicted values are mostly in agreement with experimental intensities. The exceptions are: the intensity of the 303 reflection which is absent in both models but of medium intensity in experimental patterns; and the predicted intensities of the 404 and 060 reflections are 'weak' and 'strong' while the observed intensities are 'absent' and 'medium'. The 404 and 060 intensities are discussed further in the final paragraph of this section. In order to investigate the 303 reflection discrepancy further, the unit cell structure was modified slightly while tracking the relative intensities of the 303 and 202 reflections. The experimental diffraction pattern of Fig. 2 indicates a ratio $|F_{303}|^2/|F_{202}|^2$ of close to one; therefore

Table 1
Chains A and B, and residues I–IV, refer to the diagram in Fig. 3 (adapted from Ref. [9])

Chain	Residue	x, y, z (along a, b, c directions)	N	O	C (alpha C)	C (carbonyl C)	C (side groups)
A	I	x	0.404	0.553	0.340	0.422	*0.340*
		y	0.074	0.426	0.252	0.426	*0.252*
		z	0.163	0.173	0.113	0.173	*0*
A	II	x	0.346	0.197	0.410	0.328	0.410
		y	0.574	0.926	0.752	0.926	0.752
		z	0.215	0.205	0.265	0.205	0.430
B	III	x	0.904	0.053	0.840	0.922	0.840
		y	0.926	0.574	0.748	0.574	0.748
		z	0.215	0.205	0.265	0.205	0.430
B	IV	x	0.846	0.697	0.910	0.828	*0.910*
		y	0.426	0.074	0.248	0.074	*0.248*
		z	0.163	0.173	0.113	0.173	*0*

The weak scattering by hydrogen atoms is not taken into account. The carbon atoms with positions denoted by italic print are inserted for the case of identical side groups, but are deleted for the case of dissimilar side groups.

Table 2
Dissimilar side groups; s, strong; m, medium; w, weak; a, absent; all $|F|^2$ values have been divided by four, for ease in differentiating between weak, medium and strong reflections

hkl	$\|F\|^2$ (calc.)	Relative intensity (calc.)
101	0.5	a
202	34	m
303	0.2	a
404	0.03	a
505	0.0004	a
606	1.6	w
201	260	s
002	320	s
231	9.5	w/m
031	1.8	w
060	100	s

The factor of four originates from the factor of two in expressions for the real and imaginary amplitude components *A* and *B*.

the calculated ratio should be close to one. The results of several modifications are presented in Table 5.

Two successive modifications to the unit cell structure improved the agreement between observed and calculated intensities. First—for the case of identical side groups—the carbon of residue I was shifted to a position of $x=0.33$ and the carbon of residue IV was shifted to a position of $x=1$. The resulting change in $|F_{303}|^2/|F_{202}|^2$ can be seen in Table 5 (in italic print). The second modification involved doubling the scattering factor of the side groups (i.e. taking twice the scattering factor of carbon) to simulate a bulkier side group. (This modification, where multiple atoms are superimposed, is designed to simulate the general effect of a bulkier side group on the structure factor.) These two successive changes resulted in the relative intensities shown in Table 5 (in bold type); the value of $|F_{303}|^2/|F_{202}|^2$ is close to one, in agreement with the experimental intensity. Fig. 4 shows a plot of $|F_{303}|^2/|F_{202}|^2$ for increasing bulkiness of the side groups.

Indeed, almost all predicted intensities—after these two modifications—fall in the range of experimental intensities (Tables 4 and 6). There are a few points to note, however. The value of $|F_{002}|^2$ has decreased, predicting a 'medium' rather than a 'strong' reflection; Fig. 5 and Table 7 demonstrate why. In polycrystalline patterns, the intensity of the 002 reflection appears similar to that of the 102 reflection, both 'strong'. Variations in crystal orientation or side group composition, from one crystal to the next, could have a net positive or negative effect on intensities in the polycrystalline pattern; this could explain why the 102 reflection appears 'strong', as predicted for the original cases presented in Tables 2 and 3. Another discrepancy that can be explained in the same way is the calculated 'strong' 060 reflection, where the observed reflection in the polycrystalline pattern is of 'medium' intensity. Also, the predicted 404 reflection is 'weak' while the reflection is observed to be 'absent' in the single crystal pattern. In this case, the difference could be attributed to variations in the side groups within the diffracting crystal (as demonstrated above, variations in atomic positions and scattering factors can have a significant effect on select reflections), or to dynamical effects. The kinematical structure factor calculations do not take into account dynamical effects or the effects of local imperfections in silk crystals—which will also affect intensities of reflections.

Table 3
Identical side groups; 1 carbon atom; s, strong; m, medium; w, weak; a, absent; all $|F|^2$ values have been divided by four

hkl	$\|F\|^2$ (calc.)	Relative intensity (calc.)
101	2.0	w
202	34	m
303	0.5	a
404	1.3	w
505	0.9	a
606	1.6	w
201	260	s
002	180	s
231	26	m
031	1.8	w
060	130	s

Table 4
Intensities of reflections observed; s, strong; m, medium; w, weak; vw, very weak; a, absent

hkl	Relative intensity (obs.)
101	(Hidden)
202	m
303	m
404	a
505	a/vw
606	w
201	s
002	s
231	w/m
031	w
060	m

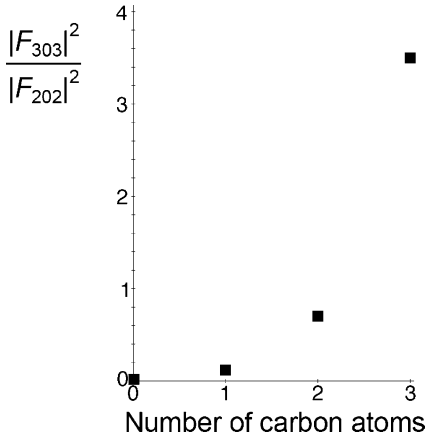

Fig. 4. A plot of $|F_{303}|^2/|F_{202}|^2$ for increasing bulkiness of side groups.

Table 5
Modifications to the crystal structure and the resulting changes to relative intensities of 202 and 303 reflections

Positions and identity of side groups	Number of carbon atoms accounted for	$\|F_{202}\|^2$	$\|F_{303}\|^2$	$\|F_{303}\|^2/\|F_{202}\|^2$
Dissimilar side groups, positions not shifted	Residues I, IV: 2 carbons. Residues II, III: 1 carbon	34	3.8	0.11
Dissimilar side groups, shifted positions: I, $x=0.33$; IV, $x=1$	Residues I, IV: 2 carbons. Residues II, III: 1 carbon	58	26	0.45
Dissimilar side groups, shifted positions: I, $x=0.33$; IV, $x=1$	Residues I, IV: 1 carbon. Residues II, III: 2 carbons	17	2.1	0.12
Identical side groups, positions not shifted	All residues: 2 carbons	11	1.1	0.10
Identical side groups, shifted positions: I, $x=0.33$; IV, $x=1$	All residues: 0 carbon	72	0.2	0.003
Identical side groups, shifted positions: I, $x=0.33$; IV, $x=1$	*All residues: 1 carbon*	*45*	*5.3*	*0.12*
Identical side groups, shifted positions: I, $x=0.33$; IV, $x=1$	**All residues: 2 carbons**	**25**	**18**	**0.7**
Identical side groups, shifted positions: I, $x=0.33$; IV, $x=1$	All residues: 3 carbons	11	38	3.5

Note that the atomic scattering factor of carbon is doubled for the case of 2 carbons, and tripled for the case of 3 carbons. This is meant to simulate the general effect of bulkier side groups (increasing scattering factors with increasing number of carbon atoms in possible side groups). All $|F|^2$ values have been divided by four.

Table 6
Intensities expected for the case of two carbon atoms for each side group; positions shifted for residue I and IV: $x=0.33$ and $x=1$, respectively; all $|F|^2$ values have been divided by four

hkl	$\|F\|^2$ (calc.)	Relative intensity (calc.)
101	16	m
202	25	m
303	18	m
404	2.5	w
505	0.2	a
606	1.2	w
201	380	s
002	38	m
231	48	m
031	6.1	w
060	180	s

4. Conclusions

The results presented above suggest that the bulkier side groups are associated with at least some of the crystals of *L. hesperus* dragline. Imperfect crystals with areas of polyalanine and areas of larger side groups could explain the streaking and associated lattice strains seen in several single crystal diffraction patterns. The bulkier side groups may form domains, with enough order to diffract, at the boundary between crystalline and amorphous regions. However, these domains could also form entire crystals, or crystals with inclusions of polyalanine regions. The ability of this material to form crystalline regions that accommodate some of the larger amino acid side groups, in addition to alanine, and thus to achieve higher percentages of crystallinity, is likely to be an important contributing factor to the high strength and toughness of this polymer.

This study also demonstrates how sensitive the predicted electron diffraction intensities are to a slight change in side group position as well as the bulkiness of the side group. Because the model includes several approximations, the detailed conclusions that can be drawn concerning the position

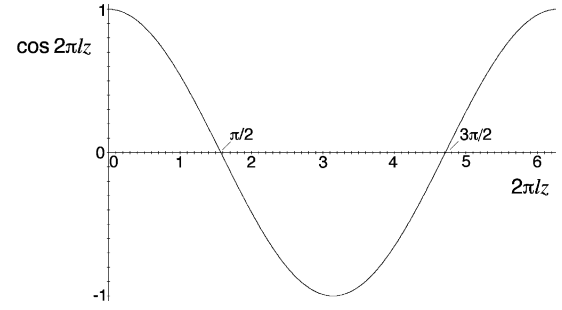

Fig. 5. For the reflection 002, $|F|^2 = A^2 = \left(\sum_j f_j \cos 2\pi l z_j\right)^2$. Note that $\cos 2\pi l z_j < 0$ for $\pi/2 < 2\pi l z_j < 3\pi/2$ (i.e. for $0.25 < l z_j < 0.75$); and $\cos 2\pi l z_j > 0$ for $2\pi l z_j < \pi/2$ and $2\pi l z_j > 3\pi/2$ (i.e. for $l z_j < 0.25$ and $l z_j > 0.75$). Therefore, with the exception of the two carbon atoms at $z=0.113$, the individual contributions of the chain (backbone) atoms to F_{002} must be negative, while the contributions of all the side group atoms must be positive (Table 7). By increasing the atomic scattering factors for the side groups, the structure factor for this reflection decreases, as expected.

Table 7
Atom positions for calculating $|F_{002}|^2$; side group atoms in italic

Atom identity	z_j	$lz_j = 2z_j$
N	0.163	0.326
N	0.215	0.430
N	0.215	0.430
N	0.163	0.326
O	0.173	0.346
O	0.205	0.410
O	0.205	0.410
O	0.173	0.346
C (alpha C)	0.113	0.226
C (alpha C)	0.265	0.530
C (alpha C)	0.265	0.530
C (alpha C)	0.113	0.226
C (carbonyl C)	0.173	0.346
C (carbonyl C)	0.205	0.410
C (carbonyl C)	0.205	0.410
C (carbonyl C)	0.173	0.346
C (side groups)	*0*	*0*
C (side groups)	*0.430*	*0.860*
C (side groups)	*0.430*	*0.860*
C (side groups)	*0*	*0*

Atoms and corresponding z_j are the same as in Table 1. None of the z coordinates are greater than 0.5 for the asymmetric unit under consideration; the asymmetric unit is 1/2 of the unit cell, hence the factor of 2 in expressions for the real and imaginary amplitude components A and B.

and identity of side groups in a given crystal are limited. However, the study points to a powerful and unique technique for obtaining both chemical (such as the identity of amino acid side groups) and physical (such as crystal size, crystal defects) nanostructural information from spider silk.

Acknowledgements

We thank Joseph Spagna and Anne Moore (W.M. Keck Science Center, The Claremont Colleges, Claremont, CA) for providing *L. hesperus* dragline silk collected under controlled conditions. We thank Cledwyn Merriman of the Department of Plant Sciences, University of Oxford for assistance in preparing TEM specimens. J.E.T. was supported by a Rhodes Scholarship and a National Science Foundation Graduate Fellowship during the period when this research was carried out.

References

[1] Haider M, Megeed Z, Ghandehari H. J Controlled Release 2004;95:1–26.
[2] Scheller J, Gührs K-H, Grosse F, Conrad U. Nat Biotechnol 2001;19:573–7.
[3] Lazaris A, Arcidiacono S, Huang Y, Zhou J-F, Duguay F, Chretien N, et al. Science 2002;295:472–6.
[4] Bell FI, McEwen IJ, Viney C. Nature 2002;416:37.
[5] Smith C, Ritchie J, Bell FI, McEwen IJ, Viney C. J Arachnol 2003;31:421–4.
[6] Viney C, Bell FI. Curr Opin Solid State Mater Sci 2004;8:165–71.
[7] Trancik JE, Czernuszka JT, Bell FI, Viney C. Submitted for publication.
[8] Warwicker JO. Acta Crystallogr 1954;7:565–73.
[9] Marsh RE, Corey RB, Pauling L. Biochim Biophys Acta 1955;16:1–34.
[10] Marsh RE, Corey RB, Pauling L. Acta Crystallogr 1955;8:62.
[11] Marsh RE, Corey RB, Pauling L. Acta Crystallogr 1955;8:710–5.
[12] Warwicker JO. J Mol Biol 1960;2:350–62.
[13] Warwicker JO. Biochim Biophys Acta 1961;52:319–28.
[14] Grubb DT, Jelinski LW. Macromolecules 1997;30:2860–7.
[15] Riekel C, Branden C, Craig C, Ferrero C, Heidelbach F, Muller M. Int J Biol Macromol 1999;24:179–86.
[16] van Beek JD, Hess S, Vollrath F, Meier BH. PNAS 2002;99:10266–71.
[17] Thiel BL, Kunkel DD, Viney C. Biopolymers 1994;34:1089–97.
[18] Thiel BL, Guess KB, Viney C. Biopolymers 1997;41:703–19.
[19] Trancik J, Czernuszka JT, Merriman C, Viney C. J Microsc 2001;203:235–8.
[20] Wrigley NG, Brown E, Chillingworth RK. J Microsc 1993;130:225–32.
[21] Trancik JE. Silk Microstructures. University of Oxford, DPhil Thesis. Copies available from: Customer Services, The British Library, Document Supply, Boston Spa, Wetherby, West Yorkshire, LS23 7BQ, UK; 2000. dsc-customer-services@bl.uk.
[22] Casem ML, Turner D, Houchin K. Int J Biol Macromol 1999;24:103–8.
[23] Hahn T, editor. International tables for crystallography. Space group symmetry, vol. A. Dordrecht, The Netherlands: Kluwer Academic Publishers; 1995.
[24] Wilson AJC, editor. International tables for crystallography. Mathematical, physical and chemical tables, vol. C. Dordrecht, The Netherlands: Kluwer Academic Publishers; 1995.
[25] Shmueli U, editor. International tables for crystallography. Reciprocal space, vol. B. Dordrecht, The Netherlands: Kluwer Academic Publishers; 1996.